Observed Self-Similarity of Precipitation Regimes over the Tropical Oceans

GREGORY S. ELSAESSER, CHRISTIAN D. KUMMEROW, AND TRISTAN S. L'ECUYER

Department of Atmospheric Science, Colorado State University, Fort Collins, Colorado

YUKARI N. TAKAYABU

Center for Climate System Research, University of Tokyo, Kashiwa, Chiba, and Institute of Observational Research for Global Change, Japan Agency for Marine-Earth Science and Technology, Yokosuka, Kanagawa, Japan

SHOICHI SHIGE*

Department of Aerospace Engineering, Osaka Prefecture University, Osaka, Japan

(Manuscript received 6 July 2009, in final form 3 December 2009)

ABSTRACT

A *K*-means clustering algorithm was used to classify Tropical Rainfall Measuring Mission (TRMM) Precipitation Radar (PR) scenes within 1° square patches over the tropical (15°S–15°N) oceans. Three cluster centroids or ''regimes'' that minimize the Euclidean distance metric in a five-dimensional space of standardized variables were sought [convective surface rainfall rate; ratio of convective rain to total rain; and fractions of convective echo profiles with tops in three fixed height ranges (<5, 5–9, and >9 km)]. Independent cluster computations in adjacent ocean basins return very similar clusters in terms of PR echo-top distributions, rainfall, and diabatic heating profiles. The clusters consist of shallow convection (SHAL cluster), with a unimodal distribution of PR echo tops and composite diabatic heating rates of ~2 K day^{-1} below 3 km; midlevel convection (MID-LEV cluster), with a bimodal distribution of PR echo tops and ~5 K day^{-1} heating up to about 7 km; and deeper convection (DEEP cluster), with a multimodal distribution of PR echo tops and >20 K day^{-1} heating from 5 to 10 km. Each contributes roughly 20%–40% in terms of total tropical rainfall, but with MID-LEV clusters especially enhanced in the Indian and Atlantic sectors, SHAL relatively enhanced in the central and east Pacific, and DEEP most prominent in the western Pacific. While the clusters themselves are quite similar in rainfall and heating, specific cloud types defined according to the PR echo top and surface rainfall rate are less similar and exhibit systematic differences from one cluster to another, implying that the degree to which precipitation structures are similar decreases when one considers individual precipitating clouds as repeating tropical structures instead of larger-scale cluster ensembles themselves.

1. Introduction

A variety of precipitating clouds, categorized by their vertical extent and rainfall characteristics, have been observed over the tropical oceans (e.g., Warren et al. 1985; Masunaga and Kummerow 2006). Even though the distribution of precipitating clouds is continuous in nature, a number of studies have consistently shown that dominant ones emerge from the spectrum: three convective types, consisting of shallow cumuli, congestus cumuli, and deep precipitating cumulonimbi (Johnson et al. 1999), and a nonconvective stratiform type, considered to be, in large, a by-product of deep convective activity in the tropics (Houze 1997). Given a particular basin, the longer-term temporal mean state of precipitating convection can be thought of as comprising the average prevalence of each convective and the attendant stratiform precipitating cloud type. Over the past few decades, satellite and in situ studies have sought to document both the mean characteristics of precipitating convection across the tropics, as well as the differences

* Current affiliation: Division of Earth and Planetary Sciences, Graduate School of Science, Kyoto University, Kitashirakawa-Oiwake-cho, Sakyo-ku, Kyoto, Japan.

Corresponding author address: Gregory Elsaesser, Department of Atmospheric Science, Colorado State University, Fort Collins, CO 80523-1371.
E-mail: elsaesser@atmos.colostate.edu

DOI: 10.1175/2010JCLI3330.1

that exist from one basin to another. Consistently, a number of observational studies have shown that the statistical average heating rate, rainfall rate, cloud fraction, cloud type, and spatial extent of rainfall systems is not homogeneous across the tropical oceans (e.g., Houze and Betts 1981; Berg et al. 2002; Masunaga and Kummerow 2006; Zuidema and Mapes 2008).

Despite the documented dissimilarities in the mean precipitation states, uncertainty remains regarding the extent to which a particular precipitation regime (containing a particular distribution of precipitating clouds) occurring in one geographic basin resembles the same regime type occurring in another basin. Specifically, it remains unclear whether or not the proportions of each cloud type (shallow precipitating cumulus, congestus, and deep convective) are approximately constant given the presence of a particular precipitation regime, to what extent precipitation regimes are mixed in terms of cloud types, and how similar particular precipitating cloud types are from one basin and one precipitation regime to another.

There is continued motivation, then, to determine whether or not precipitation regimes can be described from an instantaneous perspective with universal descriptors versus describing precipitation from a longer temporal mean perspective. This study explores the nature of precipitation regimes through consideration of the ensemble of precipitating clouds (beyond the most prevalent cloud type) belonging to a precipitation regime, with further investigation into how consistent each regime's spectral cloud ensemble is as a function of a tropical ocean basin. Precipitation regimes are objectively identified and characterized using a common clustering framework applied separately and independently to adjacent geographic basins spanning the entire tropics, with the intention of diagnosing the extent to which regimes are similar. It is assumed a priori that regimes contain a mixture of precipitating cloud types and, therefore, individual precipitating clouds are not isolated so as to avoid compositing similar precipitating clouds from different regimes. The role of each cloud type within the precipitation regimes, in terms of their contribution to regime diabatic heating, is also investigated using new satellite-based products.

Results are presented that support a stronger idea of precipitation regime self-similarity by considering a regime comprising an ensemble of precipitating clouds as a whole, rather than considering precipitating clouds independent of the precipitation regime in which they are developing. These precipitation regimes in their entirety may better serve as repeatable, recurring "building blocks" of the mean state of tropical precipitation instead of considering individual precipitating clouds as the building blocks themselves.

2. Data sources

The primary data products used are derived from instruments onboard the Tropical Rainfall Measuring Mission (TRMM) satellite. The period of study consists of 24 months from June 2006 to May 2008. Both TRMM Precipitation Radar (PR) attenuation-corrected radar reflectivity (Z_E) profiles (surface to 20 km) and surface rainfall rates at the PR native spatial resolution (approximately 5 km) are used and are provided in the standard TRMM PR 2A25 product (hereafter the 2A25 product; Iguchi et al. 2000). For each PR pixel classified as convective, the precipitation-top height (PTH) corresponding to the observed precipitating cloud is computed. The PTH is the altitude of the highest radar echo above the earth's surface with a reflectivity of at least 17 dBZ (further details in Short and Nakamura 2000). A new dataset is created, with a 1° horizontal resolution centered on nadir PR pixels for all TRMM orbits, where each sample now comprises all PTHs associated with the spectrum of precipitating convective clouds that are present in the 1° grid. The decision is made to consider the distribution of PTHs within a 1° grid for the following three primary reasons: 1) the root-mean-square (RMS) error variances in the ancillary diabatic heating products decrease as the spatial averaging widths increase; 2) the desire to capture the statistical distribution of cloud PTHs present at some instantaneous time in a larger-scale regime requires the consideration of larger box widths; and 3) the nature of the PR scan geometry leads to an undersampling of shallow cloud PTHs for pixels significantly off-nadir, and, therefore, a coarser-than-1° resolution leads to PTH distributions that are biased with respect to the number of shallow precipitating clouds that are present. The average rainfall rate for each type of precipitating convective cloud, the average stratiform rainfall rate, diabatic heating, and the number of nonconvective and nonraining pixels are also stored for each 1° sample.

The apparent heat source (Q_1; Yanai et al. 1973) is the diabatic heating associated with unresolved cloud processes occurring in a rainfall regime. Here, Q_1 can be written as

$$Q_1 = \frac{\partial}{\partial t}\overline{s} + \nabla \cdot (\overline{s}\,\overline{\mathbf{V}}) + \frac{\partial}{\partial p}\overline{s}\,\overline{\omega} = \overline{Q_R} + \overline{\mathrm{LH}} - \frac{\partial}{\partial p}\overline{s'\omega'}, \tag{1}$$

where the total change in the dry static energy ($s = c_pT + gz$), horizontally averaged over a specified domain size (as indicated by the overbar), is given by the sum of three horizontally averaged diabatic heating components: the radiative heating rate (Q_R), the latent heating rate resulting from phase changes of water (LH), and the

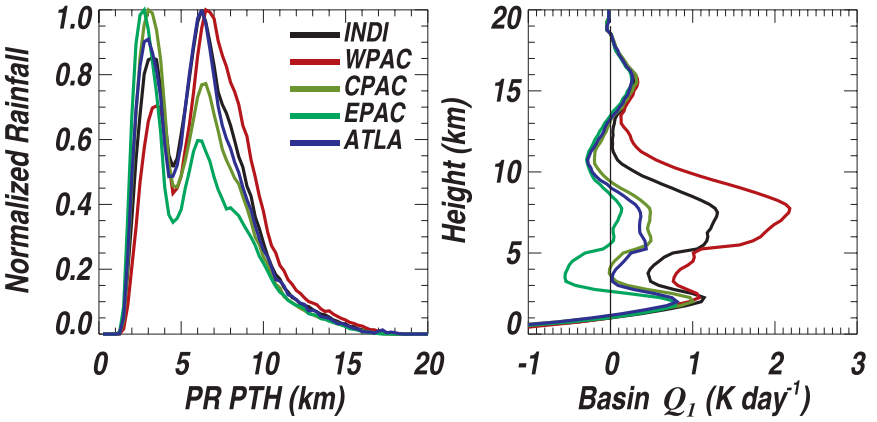

FIG. 1. (left) The distribution of rainfall as a function of convective cloud PTH for basins spanning the tropical oceans. Distributions are normalized to account for differences in total rainfall in each basin (see text for further description). (right) The average Q_1 profile for each basin is illustrated.

heating resulting from vertical eddy heat flux ($\overline{s'\omega'}$) convergence (the primes indicate a departure from a horizontal mean). A term incorporating the effects of horizontal eddy heat fluxes is assumed to be small, and has not been derived. The spectral latent heating algorithm product (SLH product; Shige et al. 2004, 2007) is used for quantification of the latter two components of the right-hand side of Eq. (1). These combined components are mathematically equivalent to $Q_1 - Q_R$ (occasionally referred to as Q_{1-R}). Heating profiles are available for each TRMM PR pixel at the PR native resolution. The SLH algorithm takes into account the vertical extent of the convection and is therefore able to differentiate shallower heating structures from deeper heating structures corresponding to various vertically extended precipitating clouds. It is important to note that the SLH algorithm estimates heating resulting from precipitation processes only, as discussed in Shige et al. (2007). The Q_{1-R} is averaged to the same 1° grids described above, and the heating profile represents the composite effect of the various precipitating clouds that are present in a rainfall regime. Horizontal averaging also has the effect of reducing the RMS error variance associated with the heating estimates (Shige et al. 2007).

The Hydrologic Cycle and Earth Radiation Budget (HERB) algorithm produces radiative heating profiles (Q_R) at 0.25° horizontal resolution and 1-km vertical resolution (L'Ecuyer and Stephens 2003, 2007; L'Ecuyer and McGarragh 2010). The algorithm utilizes cloud and precipitation information in conjunction with atmospheric water vapor, temperature profiles, and surface variables derived using sensors onboard the TRMM satellite, and incorporates a radiative transfer model that simulates vertical profiles of longwave (LW) and shortwave (SW) radiative fluxes. Heating rates are then derived using radiative flux divergences, and these estimates are averaged to 1° [these represent the first term on the right-hand side of Eq. (1)]. Only data from June 2006–December 2007 are used in this study because the satellite data from January 2008 onward are not yet processed. The vertical profiles of Q_R are smoothed using a 3-km boxcar-averaging window because the nominal 1-km vertical resolution of the product is likely coarser due to the sole use of passive remote sensing techniques for determining cloud boundaries in the algorithm (L'Ecuyer and McGarragh 2010).

3. Precipitation regime identification and self-similarity

Figure 1 shows the temporal mean state of precipitation and the associated Q_1 for five adjacent geographic regions spanning the tropics for the time period under study. These five regions extend meridionally from 15°S to 15°N over the tropical oceans and are labeled according to the ocean basin they predominantly encompass [see Fig. 4; Indian (INDI), west Pacific (WPAC), central Pacific (CPAC), east Pacific (EPAC) and Atlantic (ATLA)]. Zonally, INDI extends from 30°–100°E, WPAC from 100°–170°E, CPAC from 170°–220°E, EPAC from 220°–290°E, and ATLA from 290°–360°E longitude. It is from this background mean precipitation state that prevalent precipitation clusters or ''regimes'' are extracted.

The left panel of Fig. 1 shows the normalized rainfall histograms as a function of cloud PTH. Histograms have been normalized as in Berg et al. (2002, their Fig. 8), such that the maximum rainfall value is equal to 1 and the area under the rainfall curve is the same for each basin. In the average sense, because the total accumulated rainfall is quite different for each basin, normalizing in this manner allows for the easier comparison of rainfall

histograms and allows one to determine which cloud types play the largest role in rainfall accumulation for each basin. Upon inspection of Fig. 1, it becomes clear that rainfall distributions for various tropical basins are neither simply scaled by a constant nor are they unimodal. There is a distinct shift in the types of precipitating clouds that produce most of the rainfall as one traverses geographic basins in the tropics. Because the majority of the rain falls from deeper clouds in the Indian and west Pacific basins (left panel of Fig. 1), one would expect that Q_1, on average, is larger in magnitude at higher altitudes compared to the other basins, a result that is seen in the right panel of Fig. 1. Like the rainfall histograms, Q_1 profiles are not unimodal either, with peak heating near 2 and 6–8 km. These results are consistent with the studies summarized in section 1 noting differences in rainfall and heating across the tropics, as well as the differences in the numbers of various precipitating cloud types across the tropical oceans.

The focus now turns toward determining if dominant precipitation clusters can be extracted from the mean state. Precipitation clusters are identified through the use of a simple *K*-means clustering algorithm (Anderberg 1973). A number of recent studies (Jakob and Tselioudis 2003; Boccippio et al. 2004; Jakob et al. 2005; Rossow et al. 2005; Zhang et al. 2007; Caine et al. 2009) used this same technique to identify cloud and precipitation regimes, and the results show the usefulness of the technique. A cluster is assumed to always contain a spectrum of precipitation clouds. To capture the ensemble, the *K*-means algorithm is applied to five variables in each 1° grid box: the number of clouds with PTHs less than 5 km, the number of clouds with PTHs from 5 to 9 km, the number of clouds with PTHs greater than 9 km, the convective rainfall rate averaged over all pixels identified as convective, and the ratio of the average convective rainfall rate to the average rainfall rate (defined as the average over all of the raining pixels). The first three variables are normalized by the number of convective precipitation pixels in the grid box. All five variables are standardized, and the *K*-means algorithm is then applied to all 1° grid samples for each ocean basin (independently) across the tropics. The algorithm seeks to find the centers of natural clusters present in a dataset. One begins by specifying both the number of clusters and the initial data centers (termed centroids, and they are chosen at random). The technique involves assigning each 1°-grid (a data point) membership to a particular cluster based on a minimum Euclidean distance measure. The distance is defined as the sum of the squared differences between each centroid variable and the same variable corresponding to the data point. After evaluating the entire dataset, centroids are recomputed by computing the new mean of each variable for all data points belonging to a particular cluster. The algorithm proceeds in an iterative manner, and when the centroid of the current iteration is the same as that of the previous iteration (decided based on the sum of the squared differences in the centroid variables from one iteration to the next), the specified convergence criterion is met and a solution is found.

a. Regime cloud-top distributions and rainfall

Three precipitation clusters emerge in each basin; together, they explain approximately 60% of the variation in the five clustering variables across the tropical oceans, a magnitude that is consistent for each geographic basin. The percent of explained variance increases much less rapidly upon the consideration of additional clusters; therefore, the a priori choice of the three clusters is considered reasonable. Over 100 iterations of the clustering algorithm were executed for each ocean basin, using a random assignment for first-guess centroids each time. The precipitation clusters were found to be largely invariant to the initial centroid assignment, providing a heuristic measure of the robustness of the results.

Figure 2 shows the relative frequency of occurrence (RFO) distributions for clouds of given PTHs for the three clusters. While a cluster is classified based on the predominant, most vertically extended precipitating cloud, each cluster consistently contains a spectrum of precipitating clouds. The shallow (SHAL) precipitation cluster in the top panel of Fig. 2 is largely unimodal, and contains precipitating clouds with PTHs peaking in the 2–3-km altitude range, with very few clouds having PTHs extending beyond 5 km. The cluster in the middle panel of Fig. 2 is consistently bimodal in all basins, with a peak in cloud PTHs near 3 km, and a prevalence of precipitating clouds with PTHs extending from 5.5 to 9 km. This is classified as a congestus precipitation (MID-LEV) cluster and is so chosen based on the definition of precipitating congestus clouds provided by Johnson et al. (1999)—namely, that congestus clouds are classified as such if their cloud tops range from 5 to 9 km. The final precipitation cluster (classified as DEEP) consists of a shallow cloud PTH peak near 3 km, and a broad second PTH peak extending in height up to 16 km, implying the existence of numerous congestus and progressively deeper precipitating clouds. It should be noted that the distributions of precipitating clouds in Fig. 2 are fairly insensitive to the current choice of PTH bin limits used for the first three clustering variables described in the previous section. For each cluster, the convective rain fractions can be determined by summing all of the RFO values for each convective cloud type (identified based on the cloud's PTH) shown in Fig. 2. These fractions are show in Table 1.

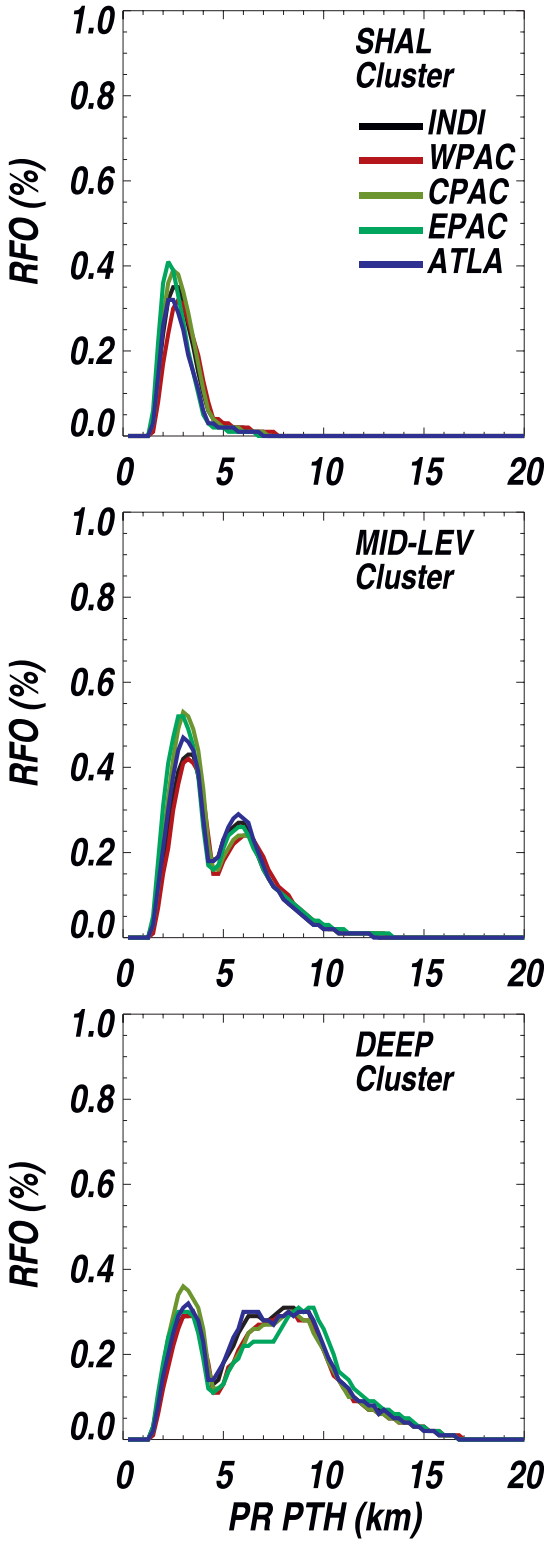

FIG. 2. The distributions of PTH for the precipitating cloud ensembles that characterize the SHAL, MID-LEV, and DEEP precipitation clusters for all tropical ocean basins. The RFO is computed by dividing the number of clouds with a given PTH by the number of pixels within each grid box.

TABLE 1. Rainfall and heating characteristics of precipitation clusters.

	SHAL	MID-LEV	DEEP
Convective rain fraction (%)	2.7	7.1	9.9
Rain fraction (%)	4.5	17.8	43.8
Average surface rainfall (mm h^{-1})	2.1	14.2	53.9
% of surface rainfall classified as stratiform	30	40	50
$\langle Q_1 - Q_R \rangle$ (K day^{-1})	0.4	3.1	12.7
$\langle Q_R \rangle$ (K day^{-1})	−1.2	−0.8	−0.3

While it has been discussed that the number of precipitating clouds stratified by cloud PTH varies across the tropics, the distributions of precipitating clouds are approximately constant within each cluster, independent of the basin under study (Fig. 2). Additionally, the MID-LEV and DEEP clusters are similar in distribution and are multimodal for all basins, with one mode consisting of prevalent warm-rain clouds topping out below the mean freezing level in the tropics, in close proximity to deeper precipitating clouds. The average rainfall fractions (defined as the total number of raining pixels divided by the total number of pixels in a grid box) are shown in Table 1. The variations of both the convective and total rainfall fractions with respect to the cluster average magnitudes are on the order of 5%, further implying that the ratio of stratiform-to-convective rain fraction is approximately the same for each cluster as a function of ocean basin, as well.

The distribution of convective rainfall parsed by PTH for each cluster and each geographic basin is shown in Fig. 3. The data analysis illustrated here is exactly the same as that illustrated in the left panel of Fig. 1, except the focus is shifted to a comparison of separate precipitation clusters for each geographic basin, and not the geographic basin in its entirety (irrespective of precipitation cluster present). Whereas the rainfall distributions are quite different in the mean sense (Fig. 1), the distributions track each other quite closely within each cluster, and the dominant peaks for convective rainfall production are quite similar for each basin given the presence of a particular cluster. These peaks are around 2–3 km for the SHAL cluster, 6–7 km for the MID-LEV cluster, and 8–9 km for the DEEP cluster. The shallower precipitating clouds (associated with PTHs extending from 3 to 4 km) that contribute to the bimodality in the PTH distribution in the MID-LEV and DEEP clusters also contribute to the bimodal rainfall histograms as well, although the peaks are less pronounced.

In the time mean sense, the average surface rainfall rate for 1° grids in each geographic basin varies, on average, by approximately 30% with respect to the tropical average surface rainfall rate (this average includes all

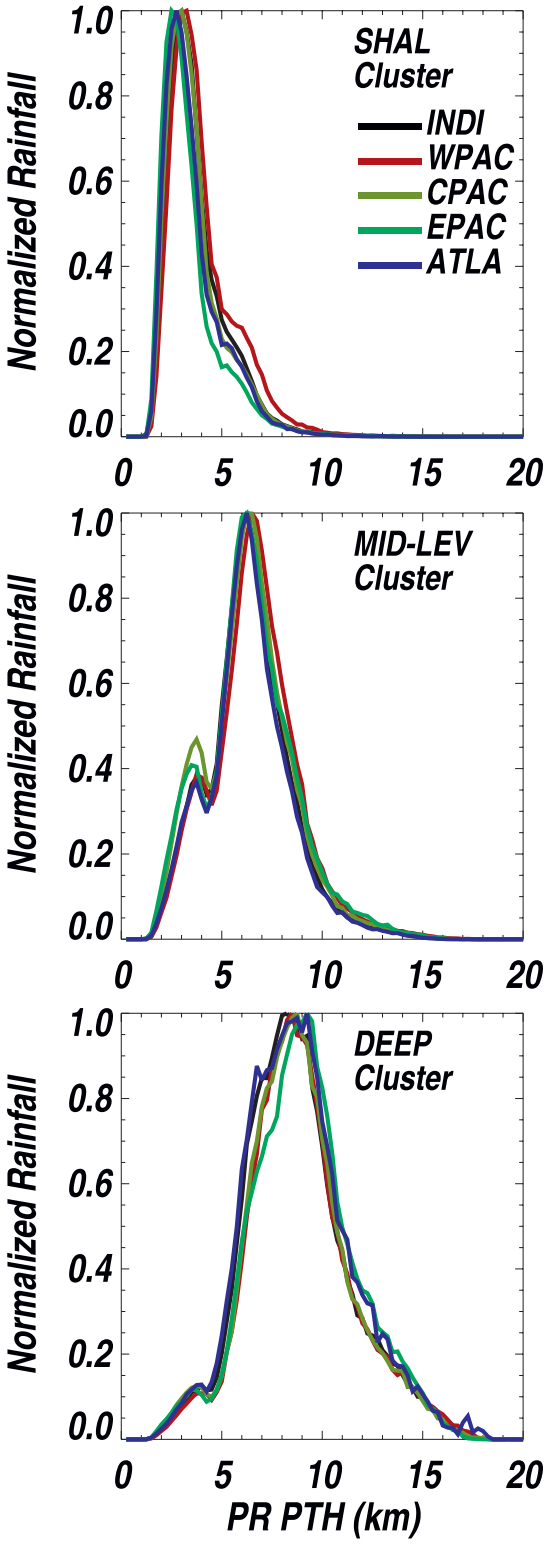

FIG. 3. As in the top panel of Fig. 1, but the rainfall distributions are now stratified by a precipitation cluster observed in each geographic basin.

1° grids, so nonraining grids are included as well). If nonraining grids are neglected, the average difference decreases to approximately 16%, so a significant percentage of the average variation arises from notable differences in the number of nonraining scenes that exist in each basin. When stratifying by cluster, however, the rainfall-rate differences are typically under 5% for all basins with respect to the cluster mean. The cluster average surface rainfall rates are provided in Table 1.

For all grid boxes covering the tropical oceans, the various cluster contributions to total accumulated rainfall are shown in the top three panels of Fig. 4. The SHAL cluster contributes 20%–25% of the total rainfall in both the INDI and WPAC regions, and as one approaches the date line and continues eastward, the SHAL cluster progressively contributes more toward the net accumulated rainfall. In the EPAC basin, the SHAL cluster contributes almost as much rainfall as the MID-LEV cluster, and more than the DEEP cluster. MID-LEV and DEEP clusters are observed everywhere throughout the tropics, including outside of the intertropical convergence zone (ITCZ) regions, and, not surprisingly, contribute significantly to the total rainfall in each geographic basin.

b. Regime diabatic heating

The Q_{1-R} profiles for the three clusters are shown in Fig. 5. Qualitatively, the profiles are quite similar for each basin, and as the intensity of convection increases, corresponding to a transition from SHAL to MID-LEV to DEEP clusters, the peak and magnitude of Q_{1-R} increases. The convective (stratiform) Q_{1-R} is the mean of the convective (stratiform) Q_{1-R} profiles corresponding to each convective (stratiform) precipitating cloud present in the cluster. As the strength of the convection increases, corresponding to stronger and deeper convective clouds, the anvil production of rainfall increases, and so does the stratiform signature of Q_{1-R}. The stratiform signature is an order of magnitude smaller in the SHAL cluster compared to the DEEP cluster. Because of the fact that stratiform rainfall production in the tropics is considered primarily to be the result of convective activity (when considering a large enough spatial scale), a sole stratiform rainfall cluster is not observed in this study. Therefore, the issue could arise where stratiform rainfall is significant outside of our identified clusters, far removed from convective towers. The right panel of Fig. 5 shows that the Q_{1-R} profiles associated with the residual stratiform rainfall for each geographic basin is quite small. The column-averaged (defined from the ocean surface to approximately 18 km) Q_{1-R} magnitudes for the residual (or unclassified) locations are approximately 0.03 K day^{-1}. This is more than an order of magnitude

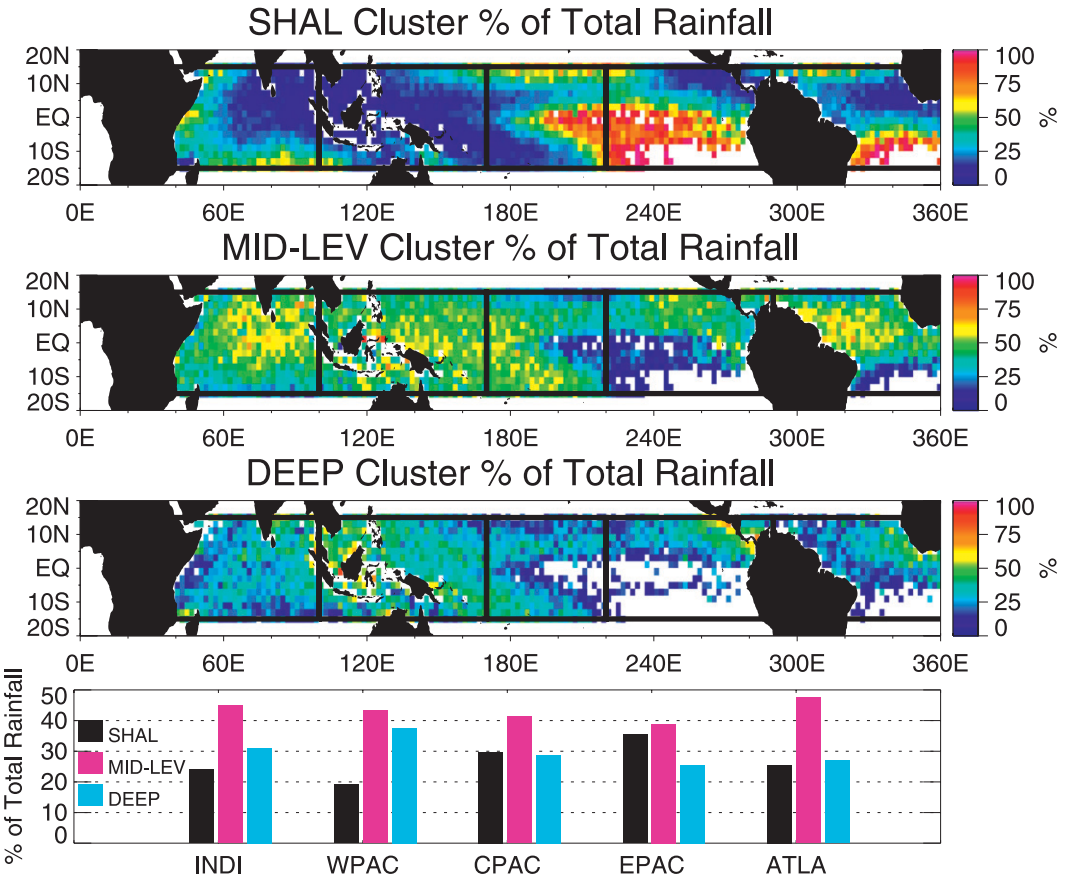

FIG. 4. (from top to bottom) The percent contribution to the total accumulated rainfall by each precipitation cluster as a function of ocean location; and, considering the five large geographic basins in their entirety, the percent contribution to the total rainfall by each cluster.

smaller than the average SHAL cluster column-averaged stratiform and convective Q_{1-R} combined. Considering that these samples make up less than 10% of the number of raining samples, the contribution to total rainfall and Q_{1-R} is minimal.

The total Q_{1-R} for each cluster and each basin is shown in Fig. 6, and is mathematically equivalent to the addition of the convective and stratiform components in each precipitation cluster. The column-averaged total Q_{1-R} magnitudes for the clusters are provided in Table 1. Regarding the profile characteristics, the SHAL cluster Q_{1-R} peaks near 2 km (Fig. 6, center panel), and the total Q_{1-R} profiles in the MID-LEV and DEEP clusters peak much higher in the atmosphere (6–8 km for the DEEP cluster). These peaks are both consistent in magnitude and altitude across all tropical ocean basins.

The radiative heating (Q_R) profiles for all clusters and basins are shown in the left panel of Fig. 6. Because the HERB Q_R algorithm uses additional, independent satellite observations for the cloud field characteristics and geometry, investigating the Q_R profiles for each cluster and for all basins can provide additional insight into the similarity of precipitation clusters. As the precipitation cluster becomes deeper, the cooling below about 11 km decreases in magnitude, likely resulting from the effect of increasing cloud cover at all altitudes leading to a decrease in the radiative flux divergences. Near the surface, as the intensity of the cluster increases (from SHAL to DEEP), Q_R rapidly approaches 0 K day^{-1}, presumably because of an increasing peak in total cloud cover in the lowest levels of the atmosphere (which is typical of more convectively active regimes), and the associated increasing downward-directed LW flux. The opposite trend occurs above 11 km, where radiative cooling increases as the cluster becomes deeper, likely resulting from the increasing cloud and anvil coverage in the 10–15-km range and the associated LW cooling to space that occurs in the vicinity of higher cloud tops. Increased cooling in the DEEP cluster aloft could also be due to increased upper-tropospheric water vapor associated with detraining deep convection leading to increased LW emission. The column-averaged Q_R

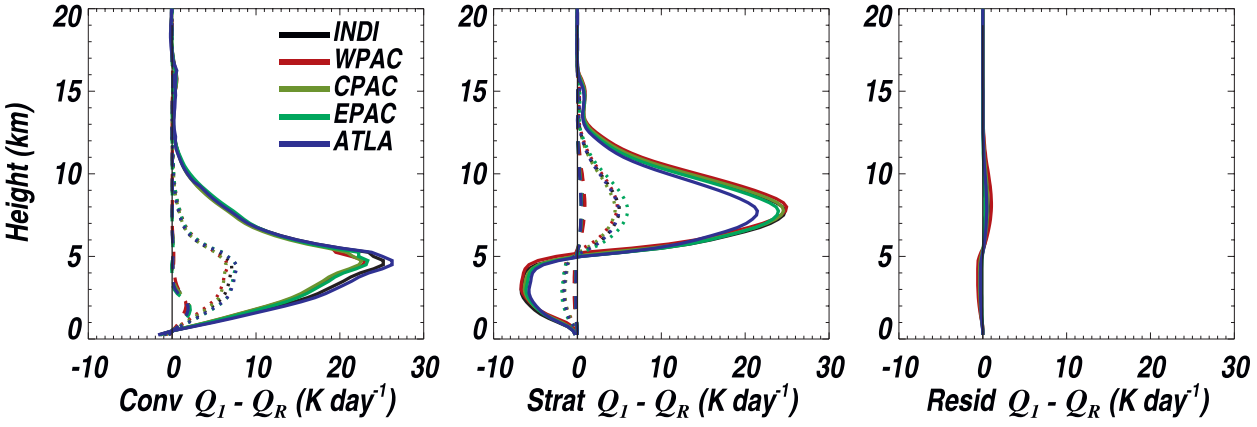

FIG. 5. The composite (left) convective and (middle) stratiform $Q_1 - Q_R$ profiles for each of the precipitation clusters and each geographic basin, and (right) the residual $Q_1 - Q_R$ profiles that remain unclassified for each basin. The SHAL (dashed), MID-LEV (dotted), and DEEP (solid) clusters are denoted in the left and middle panels.

magnitudes are shown in Table 1. These Q_R magnitudes are quite different from each other, suggesting significant differences in the cloud fields from one cluster to another. However, the average differences of these magnitudes with respect to the cluster-stratified Q_R magnitudes are on the order of 5% for all basins. This implies that given the presence of a particular precipitation cluster, the cloud fields across the tropical geographic basins are fairly similar.

Given the Q_R and Q_{1-R} components of diabatic heating, the apparent heat source Q_1 can now be quantified for each cluster and basin (Fig. 6). In heavily precipitating clusters Q_{1-R} is much larger in magnitude than Q_R (resulting from the effects of latent heating), and therefore Q_R serves to only slightly shift (negative direction) the Q_{1-R} profiles for the MID-LEV and DEEP clusters; in contrast, Q_R has a larger impact in the weakly convecting SHAL clusters because Q_{1-R} is comparable in magnitude. In these commonly observed SHAL clusters, Q_1 shows cooling throughout the troposphere above 2–3 km, and warming below resulting from the action of precipitating shallow cumulus clouds.

Provided with the relative frequency of occurrence of each cluster as a function of geographic basin, one can now assess the contribution each cluster makes toward the statistical basin-averaged Q_1 profiles (bottom panel of Fig. 1). The 2-km peak in Q_1, which is evident in all basins, is largely the result of the unimodal SHAL clusters being present in most tropical oceanic locations. Specifically, 80% of the magnitude of this peak can be attributed to the SHAL clusters (top panel of Fig. 7), which is a consistent result seen from one basin to the next. The next peak in Q_1, centered near 8 km, is contributed to heavily and almost equally by all clusters. The warming by convection in the MID-LEV and DEEP clusters contributes positively to this peak, while radiative cooling

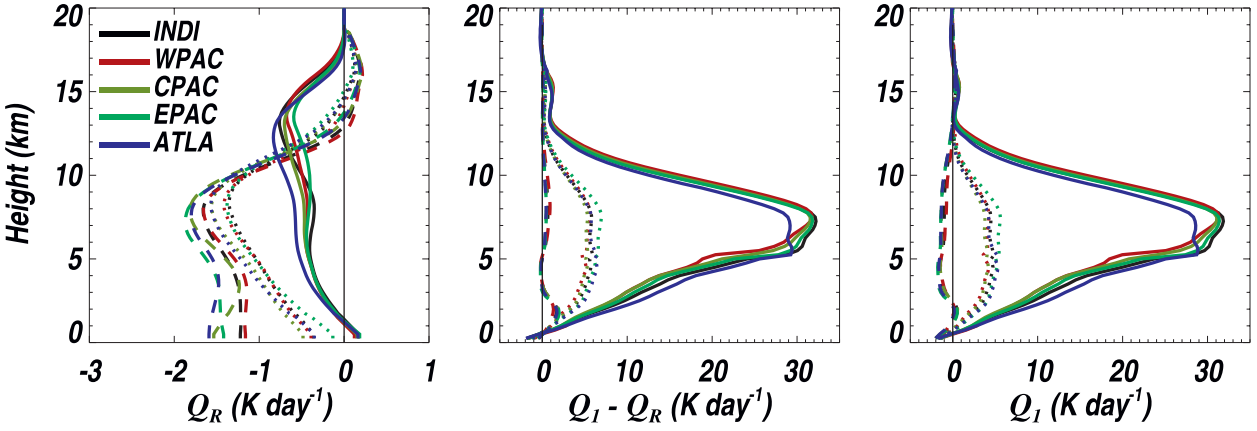

FIG. 6. The (left) Q_R, (middle) $Q_1 - Q_R$, and (right) Q_1 profiles for each of the precipitation clusters and basins are shown. The clusters are indicated according to line style as in Fig. 5.

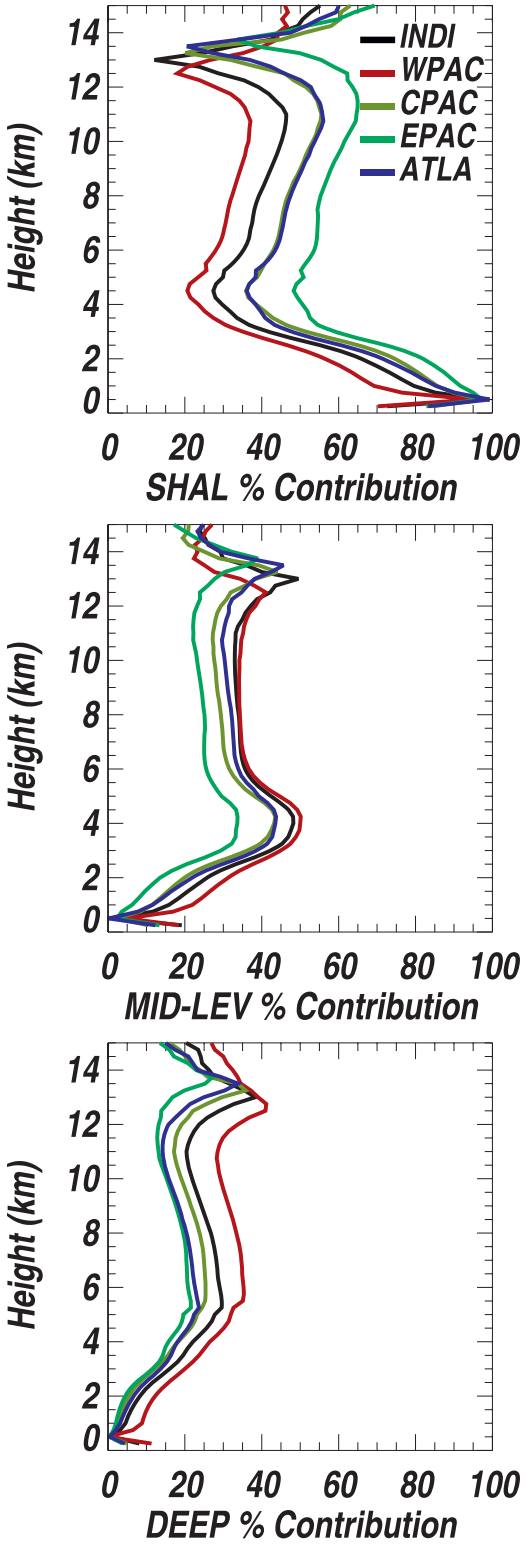

FIG. 7. The percent contribution to the average Q_1 by each precipitation cluster (as a function of altitude) for each ocean basin.

in the SHAL clusters contributes negatively and decrease the magnitude of this peak. Because deeper clusters are less prevalent in the eastern Pacific and Atlantic Oceans, the Q_1 magnitude at this altitude is closer to 0 K day^{-1} (Fig. 1) because radiative cooling from the SHAL clusters overwhelms the heating by the less prevalent deeper convective clusters.

c. *Cloud-type contributions to cluster Q_1 profiles*

While a precipitation cluster is characterized according to the most prominent, vertically extended cloud type, other precipitating cloud types consistently coexist in the deeper clusters. There are three prominent peaks in convective cloud PTHs that are clearly seen in the bottom two panels of Fig. 2: the first peak extends from 0 to 5 km, the second from 5 to 9 km, and the third (mostly a DEEP feature) encompasses the deeper convective clouds with precipitation tops extending from 9 to 20 km. These three broad peaks are likely the result of often-observed precipitating convective clouds and can loosely be classified as precipitating shallow, congestus, and deep clouds, consistent with the definition provided by Johnson et al. (1999) and others. Because clusters have been shown to consist of well-defined cloud ensembles, independent of the basin under study, it is worthwhile to proceed with an investigation of the role each cloud type plays in terms of net heating observed in a cluster.

In the top-left panel of Fig. 8, the average MID-LEV cluster Q_1 profile is reconstructed by sequentially adding in progressively shallower precipitating convective clouds and associated Q_{1-R} profiles to the combined average stratiform Q_{1-R} and Q_R profiles that are representative of the cluster. In the top-right panel of Fig. 8, the relative importance (in terms of the percent of contribution) of the particular cloud types (stratiform, shallow, congestus, and deep convective) to the MID-LEV Q_1 profile is shown. The uppermost part of the Q_1 profile in the MID-LEV cluster (above 7 km) is mostly reproduced by the stratiform component of Q_{1-R} (see the 90% contribution by the Strat + Q_R profile in the top-right panel of Fig. 8). The lower half of Q_1 (lower than 7 km) is nearly reproduced upon the addition of the congestus cloud Q_{1-R} (40%–80% of peak is the result of heating by these clouds). Adding in the shallow convective cloud Q_{1-R} allows for a broadening of the lower portion of the profile (1–2 K day^{-1}), as indicated by comparing the dashed and solid lines in the top-left panel of Fig. 8. Heating by shallow convection is responsible for 20% of the Q_1 magnitude near the surface (the solid line in the top-right panel), with significant cooling resulting from evaporation of precipitation and radiative cooling as indicated by the Strat + Q_R profile. Shallow, congestus, and stratiform

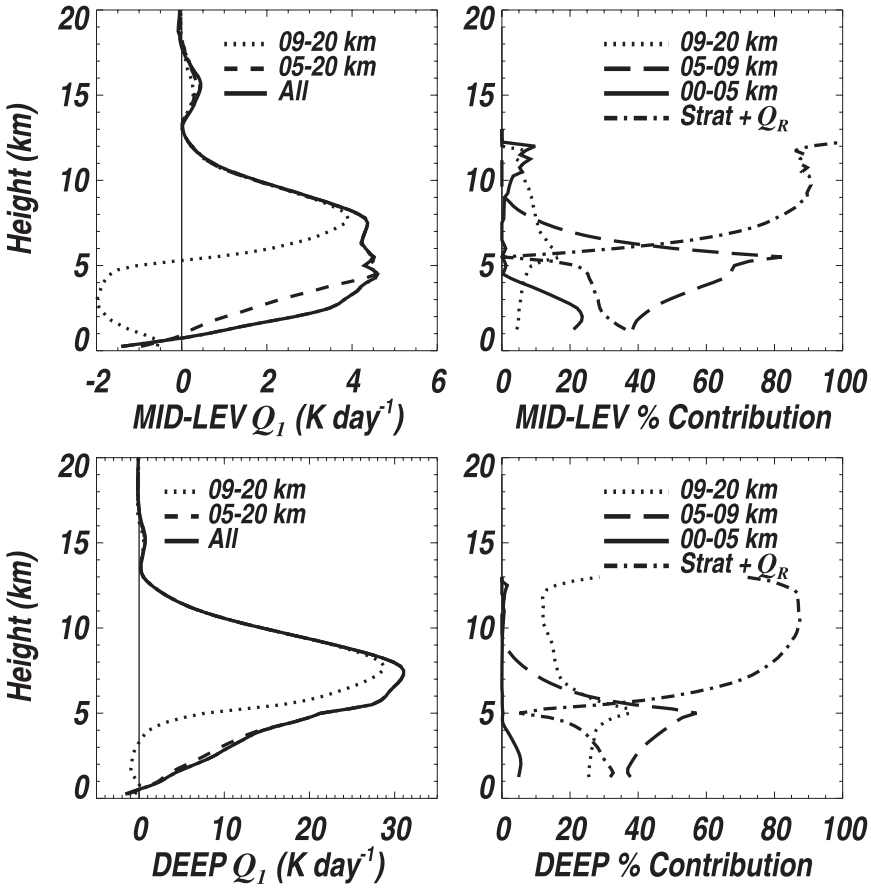

FIG. 8. The reconstruction of the average (top left) MID-LEV and (bottom left) DEEP Q_1 profiles, computed by successively adding the average convective $Q_1 - Q_R$ profiles (associated with three specified subsets of convective cloud ensembles) to the combined stratiform $Q_1 - Q_R$ and average Q_R profile characterizing the cluster. The three convective ensembles consist of clouds with PTHs ranging from 9 to 20 km (dotted), 5 to 20 km (dashed), and 1 to 20 km (solid). The contribution by cloud-type ensemble (stratiform and the three convective ensembles) to the average Q_1 profile characterizing the (top right) MID-LEV and (bottom right) DEEP clusters.

cloud types all contribute to significant but varying degrees (as a function of height) to the net MID-LEV cluster Q_1, and do so in a consistent manner for each ocean basin.

Considering now the DEEP cluster, and proceeding as before, successively shallower Q_{1-R} profiles are added to the DEEP cluster combined stratiform Q_{1-R} and Q_R profiles toward reconstruction of the cluster average Q_1. It is evident that the positive lower portion of Q_1 emerges after the congestus Q_{1-R} is taken into consideration [the congestus clouds contribute 40%–60% toward the net heating, which is slightly larger than the contribution by deeper (9–20-km PTHs) clouds]. The role of the shallower convective clouds (consisting of PTHs from 0 to 5 km) is not as significant in the DEEP cluster as in the MID-LEV one (seen by comparing dashed to solid line in bottom-left panel), contributing only slightly to the magnitude of the Q_1 profile from 1 to 4 km. The uppermost portion of DEEP Q_1 (above 7 km) is largely reproduced upon consideration of the deep convective precipitating cloud (PTHs from 9 to 20 km) and the stratiform component of heating.

4. Dissimilarity in precipitating cloud types

An attempt has been made to show that precipitation clusters are similar in appearance, with nearly indistinguishable cloud ensembles, rainfall distributions, and heating profiles. It is worth discussing whether or not the idea of self-similarity can be extended to specific precipitating cloud types. For instance, does a precipitating congestus cloud observed in one precipitation cluster look similar to that in another cluster in terms of surface rainfall rate and vertical profile of radar reflectivity? While deep convective clouds produce a significant

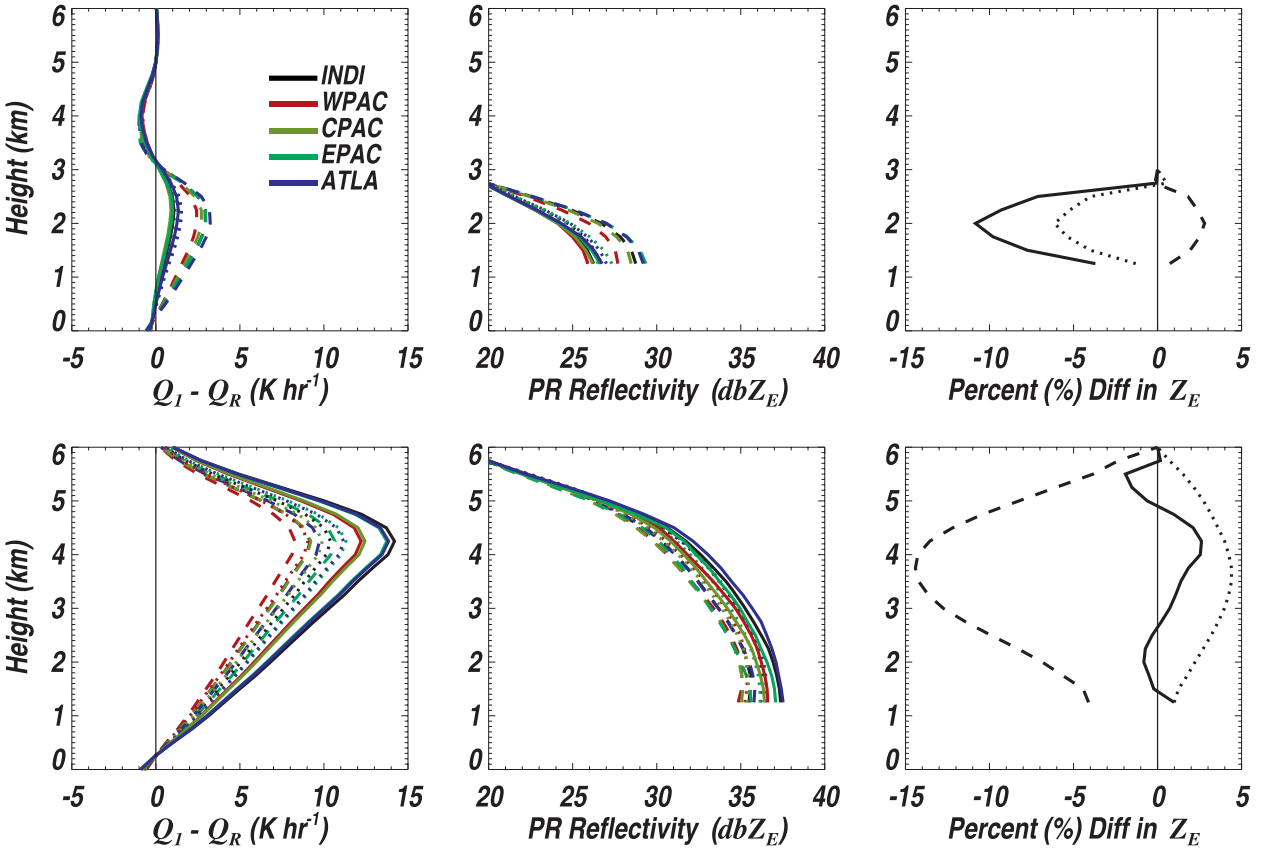

FIG. 9. (top left) The average convective $Q_1 - Q_R$ profiles for convective clouds having PTHs of 3 km for each precipitation cluster [SHAL (dashed), MID-LEV (dotted), and DEEP (solid) clusters]. (top middle) As at top left, but for the PR Z_E profiles. (top right) For each precipitation cluster (line style denotes the cluster), the percent difference in Z_E as a function of height given a convective cloud with a 3-km PTH and the same surface rainfall rate (averaged over all basins). The bottom three panels are constructed as in the top two panels, but for the precipitating clouds having PTHs of 6 km.

amount of rainfall and latent heating, shallow and congestus cloud types (defined as earlier according to their PTH distributions), resulting from their significant RFO over the tropical oceans, contribute roughly 38% and 47% of the observed total convective rainfall, respectively. Because these clouds are particularly important in terms of rainfall in the tropics, the idea of cloud-type similarity is discussed through consideration of particular precipitating clouds within the broad shallow and congestus classifications.

Consider two particular precipitating cloud types within these categories that have PTHs of 3 and 6 km. The cloud with a 3-km PTH can be considered a shallow, warm-raining cloud, while the 6-km precipitating cloud most likely extends beyond the tropical freezing level and may contain ice near the cloud top. Stratified by precipitation cluster, the average surface rainfall rate for a cloud with a 3-km PTH (at TRMM PR instantaneous resolution) is 2.1, 1.5, and 1.4 mm h^{-1} for SHAL, MID-LEV, and DEEP clusters, respectively. As the cluster becomes deeper, the strength of the 3-km precipitating clouds decrease in terms of surface rainfall rate, which is somewhat surprising, but is nonetheless consistent for all basins. Figure 9 depicts the Q_{1-R} and radar reflectivity profiles for the 3-km clouds in the top three panels. One would expect that the Q_{1-R} from these 3-km cloud types should decrease, consistent with the surface rainfall-rate trends, which is indeed what is observed. It must be noted that Q_{1-R} can be considered a larger-scale variable dependent on the precipitating cloud system as a whole, so further interpretation of the Q_{1-R} profiles would be more speculative. The top-middle panel of Fig. 9 shows the corresponding 2A25 product radar reflectivity profiles for the 3-km precipitating clouds. Consistent with the rainfall rates, as the precipitation regime grows deeper, the radar reflectivity profiles weaken for these cloud types. The Q_{1-R} and radar reflectivity profiles for the clouds with 6-km PTHs are shown in the bottom three panels of Fig. 9. For a precipitating cloud with a 6-km PTH, the average surface rainfall rate is 7.5, 8.2, and 10.7 mm h^{-1}

for SHAL, MID-LEV, and DEEP clusters, respectively. Unlike the trend for clouds with 3-km PTHs, the rainfall rate, Q_{1-R}, and radar reflectivity values increase as the clusters transition from SHAL to DEEP (bottom-left and bottom-center panels of Fig. 9). This is also qualitatively consistent from one geographic basin to the next.

If one becomes more stringent in the definition of a precipitating cloud type, such that it is now defined by both a particular vertical thickness and surface rainfall rate, then further investigation into the differences in the profiles of radar reflectivity as a function of height for the three clusters can be made. The results are averaged over all basins, and the average percent difference in radar reflectivity relative to the mean radar reflectivity profile is shown for precipitating clouds defined according to PTH and surface rainfall rate. The results can be seen in the far-right two panels of Fig. 9. Robust differences emerge, and for the 3-km clouds, given the same surface rainfall rate, there is a 14% difference in radar reflectivity at 2 km between precipitating clouds developing in the SHAL cluster versus the DEEP cluster. For the 6-km clouds, given the same surface rainfall rates once again, there is an 18% difference in radar reflectivity at 3.5 km between precipitating clouds developing in the SHAL cluster compared to those developing in the MID-LEV cluster.

It is evident that the differences between these average surface rainfall rates, Q_{1-R}, and radar reflectivity are large and highly dependent on the precipitation regime in which the cloud is developing. However, the rainfall rates are similar with respect to the tropical average surface rainfall rate for these clouds when one stratifies by precipitation cluster (less than a 7% difference from the cluster average). These results provide motivation for the study of precipitating clouds within the context of the precipitation regime in which they are developing, as opposed to considering precipitating clouds with the same vertical extent and/or rainfall characteristics as self-similar entities, independent of the precipitation regime.

5. Conclusions

A wealth of knowledge exists on the nature of tropical precipitation, both in the temporal mean sense and also with respect to the prevalence of precipitating clouds as one traverses the various ocean basins in the tropics. In this study, an analysis geared toward extracting precipitation regimes from the mean tropical state is performed, but is done so independently for adjacent ocean regions with the purpose of determining how similar various precipitation regimes are across the tropics. The framework has the advantage of not requiring, for example, the specification of how many deep precipitating clouds must exist in a regime for it to be declared ''deep'' or what percentage of stratiform/convective cloud types must exist in a given area for a particular type of regime to be defined. Three similar precipitation clusters emerge such that a particular cluster occurring in one basin is nearly indistinguishable from the same cluster identified in another basin. Clusters are quantitatively similar in terms of the ensembles of cloud types, the distributions of rainfall, and the distributions of heating resulting from the spectrum of precipitating clouds that are present. Precipitating shallow and congestus clouds are in close proximity to each other, as well as in close proximity to deep convective clouds in deeper precipitation clusters. Because a cluster contains a distribution of cloud entities that are not self-similar (despite having the same vertical extent and rainfall), studies that focus on a particular cloud type and its associated ambient thermodynamic characteristics may inadvertently mix regimes by, for example, extracting shallow clouds from a deeper convection regime and shallow clouds from a weakly convecting regime and compositing the profiles and their corresponding environmental characteristics together.

Within the deeper precipitation clusters, the distributions of PTHs are consistently bimodal. It is shown that particular ensembles of cloud types play significant roles in the composite structure of the heating profiles. These results are both robust and consistent from one tropical ocean basin to the next. Additionally, these results indicate that it may be necessary to consider the entire spectrum of precipitating that are clouds present in a particular regime in order to capture the heating profile (largely driven by the latent heating term), beyond a rainfall scaling of a generalized latent heating function that depends largely on the amount of stratiform and convective rainfall present.

It is an important result that similar precipitation clusters emerge, particularly because equatorial atmospheric wave activity frequency and large-scale dynamics vary as a function of the tropical oceanic basin. Considering that convectively coupled equatorial waves are more prevalent in some basins than others, and that the Madden–Julian oscillation (MJO) primarily influences the Indian and west Pacific Ocean basins, the result of cluster similarity in terms of the distributions of PTH, rainfall, and heating is a significant one, implying that precipitation clusters do not change regardless of the type of equatorial disturbance; rather, they are simply modulated in terms of frequency of occurrence by the disturbance.

Continued interpretation of these clusters, as well as their placement within the ''extended building block'' hypothesis recently proposed by Mapes et al. (2006), which describes a self-similar progression of precipitating

convection from shallow to deeper structures despite being modulated by different large-scale tropical waves, requires the incorporation of additional datasets describing the thermodynamic and dynamic states of the atmosphere. Furthermore, reconciling the remaining cluster differences that exist from one basin to another may require consideration of the idea that some precipitation regimes may be either terminal (i.e., they have reached their peak intensity) or transient (i.e., intensifying and growing toward a deep convective state), as discussed in Luo et al. (2009). It is possible that the same distribution of precipitating clouds could exist in either case, but there is good reason to expect that the heating and rainfall may be different between the two cases, which could provide some insight into why precipitating clouds have similar characteristics with respect to the cluster in which they are developing, but not with respect to the same cloud types developing in another cluster.

Acknowledgments. This work has been supported by the National Science Foundation Science and Technology Center for Multiscale Modeling of Atmospheric Processes (CMMAP), managed by the Colorado State University under Cooperative Agreement ATM-0425247. It was also partially supported by NASA Grant NNX07AD75G.

REFERENCES

Anderberg, M. R., 1973: *Cluster Analysis for Applications*. Academic Press, 359 pp.

Berg, W., C. D. Kummerow, and C. Morales, 2002: Differences between east and west Pacific rainfall systems. *J. Climate,* **15,** 3659–3672.

Boccippio, D. J., W. A. Petersen, and D. J. Cecil, 2004: The tropical convective spectrum. Part I: Archetypal vertical structures. *J. Climate,* **18,** 2744–2769.

Caine, S., C. Jakob, S. Siems, and P. May, 2009: Objective classification of precipitating convective regimes using a weather radar in Darwin, Australia. *Mon. Wea. Rev.,* **137,** 1585–1600.

Houze, R. A., Jr., 1997: Stratiform precipitation in regions of convection: A meteorological paradox? *Bull. Amer. Meteor. Soc.,* **78,** 2179–2196.

——, and A. K. Betts, 1981: Convection in GATE. *Rev. Geophys. Space Phys.,* **19,** 541–576.

Iguchi, T., T. Kozu, R. Meneghini, J. Awaka, and K. Okamoto, 2000: Rain-profiling algorithm for the TRMM precipitation radar. *J. Appl. Meteor.,* **39,** 2038–2052.

Jakob, C., and G. Tselioudis, 2003: Objective identification of cloud regimes in the Tropical Western Pacific. *Geophys. Res. Lett.,* **30,** 2082, doi:10.1029/2003GL018367.

——, ——, and T. Hume, 2005: The radiative, cloud, and thermodynamic properties of the major tropical western Pacific cloud regimes. *J. Climate,* **18,** 1203–1215.

Johnson, R. H., T. M. Rickenbach, S. A. Rutledge, P. E. Ciesielski, and W. H. Schubert, 1999: Trimodal characteristics of tropical convection. *J. Climate,* **12,** 2397–2418.

L'Ecuyer, T. S., and G. L. Stephens, 2003: The tropical oceanic energy budget from the TRMM perspective. Part I: Algorithm and uncertainties. *J. Climate,* **16,** 1967–1985.

——, and ——, 2007: The tropical oceanic energy budget from the TRMM perspective. Part II: Evaluating GCM representations of the sensitivity of regional energy and water cycles to the 1998–99 ENSO cycle. *J. Climate,* **20,** 4548–4571.

——, and G. McGarragh, 2010: A 10-yr climatology of tropical radiative heating and its vertical structure from TRMM observations. *J. Climate,* **23,** 519–541.

Luo, Z., G. Y. Liu, G. L. Stephens, and R. H. Johnson, 2009: Terminal versus transient cumulus congestus: A CloudSat perspective. *Geophys. Res. Lett.,* **36,** L05808, doi:10.1029/2008GL036927.

Mapes, B., S. Tulich, J. Lin, and P. Zuidema, 2006: The mesoscale convection life-cycle: Building block or prototype for large-scale tropical waves? *Dyn. Atmos. Oceans,* **42,** 3–29.

Masunaga, H., and C. D. Kummerow, 2006: Observations of tropical precipitating clouds ranging from shallow to deep convective systems. *Geophys. Res. Lett.,* **33,** L16805, doi:10.1029/2006GL026547.

Rossow, W. B., G. Tselioudis, A. Polak, and C. Jakob, 2005: Tropical climate described as a distribution of weather states indicated by distinct mesoscale cloud property mixtures. *Geophys. Res. Lett.,* **32,** L21812, doi:10.1029/2005GL024584.

Shige, S., Y. N. Takayabu, W.-K. Tao, and D. E. Johnson, 2004: Spectral retrieval of latent heating profiles from TRMM PR data. Part I: Development of a model-based algorithm. *J. Appl. Meteor.,* **43,** 1095–1113.

——, ——, ——, and C.-L. Shie, 2007: Spectral retrieval of latent heating profiles from TRMM PR data. Part II: Algorithm improvement and heating estimates over tropical ocean regions. *J. Appl. Meteor. Climatol.,* **46,** 1098–1124.

Short, D. A., and K. Nakamura, 2000: TRMM radar observations of shallow precipitation over the tropical oceans. *J. Climate,* **13,** 4107–4124.

Warren, S. G., C. J. Hahn, and J. London, 1985: Simultaneous occurrence of different cloud types. *J. Climate Appl. Meteor.,* **24,** 658–667.

Yanai, M., S. Esbensen, and J.-H. Chu, 1973: Determination of bulk properties of tropical cloud clusters from large-scale heat and moisture budgets. *J. Atmos. Sci.,* **30,** 611–627.

Zhang, Y., S. Klein, G. G. Mace, and J. Boyle, 2007: Cluster analysis of tropical clouds using CloudSat data. *Geophys. Res. Lett.,* **34,** L12813, doi:10.1029/2007GL029336.

Zuidema, P., and B. Mapes, 2008: Cloud vertical structure observed from space and ship over the Bay of Bengal and the eastern tropical Pacific. *J. Meteor. Soc. Japan,* **86A,** 205–218.